

RESEARCH PAPER



## TgATG9 is required for autophagosome biogenesis and maintenance of chronic infection in *Toxoplasma gondii*

Pariyamon Thaprawat<sup>a,b</sup>, Zhihai Zhang<sup>c</sup>, Eric C. Rentchler<sup>d</sup>,  
Fengrong Wang<sup>a</sup>, Shreya Chalasani<sup>a</sup>, Christopher J. Giuliano<sup>e,f</sup>,  
Sebastian Lourido<sup>e,f</sup>, Manlio Di Cristina<sup>g</sup>, Daniel J. Klionsky<sup>id</sup><sup>c</sup>  
and Vern B. Carruthers<sup>a</sup>

<sup>a</sup>Department of Microbiology and Immunology, University of Michigan Medical School, Ann Arbor, MI, USA; <sup>b</sup>Medical Scientist Training Program, University of Michigan Medical School, Ann Arbor, MI, USA; <sup>c</sup>Life Sciences Institute and Department of Molecular, Cellular and Developmental Biology, University of Michigan, Ann Arbor, MI, USA; <sup>d</sup>Biomedical Research Core Facilities, Microscopy Core, University of Michigan Medical School, Ann Arbor, MI, USA; <sup>e</sup>Whitehead Institute, Cambridge, USA; <sup>f</sup>Biology Department, Massachusetts Institute of Technology, Cambridge, USA; <sup>g</sup>Department of Chemistry, Biology and Biotechnology, University of Perugia, Perugia, Italy


### ABSTRACT

*Toxoplasma gondii* is a ubiquitous protozoan parasite that can reside long-term within hosts as intracellular tissue cysts comprised of chronic stage bradyzoites. To perturb chronic infection requires a better understanding of the cellular processes that mediate parasite persistence. Macroautophagy/autophagy is a catabolic and homeostatic pathway that is required for *T. gondii* chronic infection, although the molecular details of this process remain poorly understood. A key step in autophagy is the initial formation of the phagophore that sequesters cytoplasmic components and matures into a double-membraned autophagosome for delivery of the cargo to a cell's digestive organelle for degradative recycling. While *T. gondii* appears to have a reduced repertoire of autophagy proteins, it possesses a putative phospholipid scramblase, TgATG9. Through structural modeling and complementation assays, we show herein that TgATG9 can partially rescue bulk autophagy in *atg9Δ* yeast. We demonstrated the importance of TgATG9 for proper autophagosome dynamics at the subcellular level using three-dimensional live cell lattice light sheet microscopy. Conditional knockdown of TgATG9 in *T. gondii* after bradyzoite differentiation resulted in markedly reduced parasite viability. Together, our findings provide insights into the molecular dynamics of autophagosome biogenesis within an early-branching eukaryote and pinpoint the indispensable role of autophagy in maintaining *T. gondii* chronic infection.

**ARTICLE HISTORY** Received: 07 Aug 2024; Revised: 10 Sep 2024; Accepted: 03 Oct 2024

**KEYWORDS** Apicomplexa; autophagy; bradyzoite; conditional knockdown; lattice light sheet microscopy; yeast complementation

**CONTACT** Vern B. Carruthers  [vcarruth@umich.edu](mailto:vcarruth@umich.edu)  Department of Microbiology and Immunology, University of Michigan Medical School, Ann Arbor, MI, USA

 Supplemental data for this article can be accessed online at <https://doi.org/10.1080/27694127.2024.2418256>

© 2024 The Author(s). Published by Informa UK Limited, trading as Taylor & Francis Group.  
This is an Open Access article distributed under the terms of the Creative Commons Attribution License (<http://creativecommons.org/licenses/by/4.0/>), which permits unrestricted use, distribution, and reproduction in any medium, provided the original work is properly cited. The terms on which this article has been published allow the posting of the Accepted Manuscript in a repository by the author(s) or with their consent.

## Introduction

*Toxoplasma gondii* is an obligate intracellular protozoan parasite that infects a wide range of hosts including humans [1]. This ubiquitous pathogen is estimated to chronically infect up to one third of the global human population [2]. Chronic-stage parasites serve as reservoirs for reactivated disease under the setting of host immune dysfunction, which can lead to severe consequences such as encephalitis and blindness in affected host organs [2-4]. There have also been reports of reactivation in otherwise healthy individuals [5,6]. Current therapies against *T. gondii* fail to eliminate the chronic infection. Hence there is a critical need to better understand the mechanisms underlying *T. gondii* persistence and identify novel targets for intervention [7].

The slow-growing form of *T. gondii* (bradyzoite) that persists during chronic infection differentiates from the rapid-growing form (tachyzoite) upon external triggers such as the host immune response, restriction of nutrients, and other stresses [8]. Bradyzoites secrete proteins that form a resilient glycan-rich cyst wall that could limit nutrient access [9-11]. Nonetheless, bradyzoites can persist within cysts long term, which necessitates mechanisms in place for maintaining cellular homeostasis by degrading macromolecular material and recycling basic components. Previous studies have demonstrated that *T. gondii* parasites rely on a cysteine protease (TgCPL) residing within a plant-like vacuolar compartment (PLVAC) for degradation of proteinaceous material [12-14]. Bradyzoite mutants lacking TgCPL accumulate within the PLVAC autophagic material including organellar remnants and show reduced viability during the chronic infection [15]. This finding suggests that proteolytic turnover of cellular materials is critical for long-term parasite persistence.

Macroautophagy (hereafter, autophagy) is an important homeostatic pathway that facilitates turnover of cellular materials. The key steps involved in autophagy include initiation in response to cellular signals such as nutrient deprivation with nucleation of the phagophore, expansion of the phagophore to engulf its cargo, maturation into an autophagosome and delivery to a cell's digestive compartment for degradative recycling [16,17]. While the molecular mechanisms of autophagy have been extensively investigated in yeast and mammalian model organisms, far less is known about the role of autophagy in early branching eukaryotes such as *T. gondii* [18,19]. Although the autophagy machinery is conserved among eukaryotes, precisely how the apicomplexan parasite *T. gondii* performs canonical autophagy with a substantially reduced

repertoire of ATG (autophagy related) proteins (TgATGs) remains unclear [19]. Also, many of the discovered TgATGs including TgATG8 and its conjugation machinery play a non-canonical role in segregation of the apicoplast, a plastid organelle originating from a secondary endosymbiosis event that harbors several key metabolic pathways [20-23]. However, the discovery and characterization of other TgATGs involved in canonical autophagy, specifically the early autophagy pathway, remain limited. Nonetheless, one conserved protein not involved in apicoplast segregation, TgATG9, has been reported to play an essential role in bradyzoite persistence, implying that canonical autophagy is a key survival pathway for chronic-stage parasites [24,25].

Atg9/ATG9 homologs are integral membrane proteins important for expansion of the autophagic membrane through their function as a phospholipid scramblase that moves and equilibrates phospholipids from the outer to the inner leaflet of the developing phagophore [26-31]. Atg2/ATG2 proteins transfer lipids from sites such as the endoplasmic reticulum and directly interact with Atg9/ATG9 in this step of the pathway [32-34]. Atg9/ATG9 in yeast and mammalian cells principally originate from the Golgi network and endosomal compartments with recruitment to sites of autophagosome formation upon induction of autophagy [35-38]. In addition to their role as scramblases, Atg9/ATG9 proteins and vesicles also serve as important sources of seed membranes for phagophore formation [39-41]. The proper assembly of core autophagy proteins moreover depend on the role Atg9/ATG9 as organizational and lipid mobilization centers required for autophagy progression [29,42-44]. Mammalian ATG9A has also been discovered to play a role in maintaining plasma membrane integrity in cooperation with other non-autophagic protein complexes [45]. While these detailed characterizations of Atg9/ATG9 function and localization have been elucidated in yeast and mammalian systems, no analogous studies have been performed in *T. gondii*. Genetic ablation of TgATG9 in bradyzoites leads to impaired autophagosome production, ultrastructural abnormalities in the PLVAC, abnormal mitochondria, aberrant bradyzoite morphology *in vitro*, and decreased levels of chronic infection *in vivo* [25]. Because these phenotypes are observed with bradyzoites harboring a stable genetic knockout of *TgATG9*, it is not possible to distinguish if TgATG9 is only necessary soon after differentiation or is required to maintain the chronic infection after it is established.

In the current study, we sought direct evidence for the role of TgATG9 in autophagosome biogenesis through yeast complementation and 3D live-cell imaging. We utilized a conditional knockdown system to further determine the direct contribution of TgATG9 to autophagic flux and survival of bradyzoites after the establishment of the chronic stage.

## Results

### ***TgATG9 partially rescues bulk autophagy in atg9Δ knockout yeast***

To determine if TgATG9 functions analogously to other Atg9/ATG9s as a putative phospholipid scramblase, we performed yeast complementation studies and assessed the rescue of bulk autophagy in *atg9Δ* knockout yeast. The TgATG9 protein contains six transmembrane domains that share homology to other Atg9/ATG9 proteins. The transmembrane domains are often termed the “core” region that confers the functionality of scrambling lipids, while the N- and C-termini have less ordered structure [26,27,30]. We performed a structural alignment of the AlphaFold3 predicted “core” of TgATG9 (aa 273-859) and *Saccharomyces cerevisiae* (Sc)Atg9 (aa 317-764), confirming that the two proteins have very similar predicted folds for their respective transmembrane regions and trimeric structures (Figure 1A) [46]. We generated yeast expression constructs driven by either the *ScATG9* promoter (*ATG9p*) or a stronger, constitutive *ZEO1* promoter (*ZEO1p*). The full-length ScAtg9 was placed under *ATG9p* expression (“Sc” in Figure 1). The full-length TgATG9 was placed under *ZEO1p* expression (“Tg” in Figure 1). To account for the importance of the N- and C-termini in recruiting other autophagy proteins or in post-translational modifications, we generated a chimera (“Ch” in Figure 1) of TgATG9 and ScAtg9 by swapping the “core” of ScAtg9 with TgATG9, thus preserving the N- and C-termini as yeast sequences (Figure 1B) [47-49]. We validated the expression of all constructs by western blotting samples from unstarved and 24 h nitrogen-starved yeast (Figure 1C-D). We also confirmed TgATG9 expression by microscopy. We transformed ScAtg9 and TgATG9 into *atg9Δ* RFP-Atg8 or *atg1Δ atg9Δ* RFP-Atg8-expressing yeast. Atg1 is required for retrograde transport of Atg9; in *atg1Δ* strains, Atg9 tends to accumulate at the phagophore assembly site [50]. We found that within 3 h of nitrogen starvation, both ScAtg9 and TgATG9 were expressed in yeast in the presence or absence of Atg1 (Figure S1) [51].

We first wanted to assess whether introduction of the full-length TgATG9 could rescue autophagic activity in *atg9Δ* knockout yeast. Using the Pho8Δ60 assay, we quantified the relative Pho8Δ60 activity normalized to wild-type controls for *atg9Δ* knockout yeast complemented with either ScAtg9 (Sc) or TgATG9 (Tg) [52]. Under nutrient-rich conditions (YPD medium) autophagy is not induced; however, after 4 h of nitrogen starvation (SD-N), bulk autophagy is induced and can be measured. Compared to the *atg9Δ* knockout, yeast complemented with ScAtg9 and TgATG9 showed an increase in Pho8Δ60 activity, albeit not to the same levels as the wild type (Figure 2A).

To further validate this finding and to take into consideration the role of the N- and C-termini in Atg9/ATG9 function, we assessed autophagy rescue using two additional assays and included the ScAtg9/TgATG9 chimera (Ch). We quantified the level of GFP-Atg8 processing, and again showed that

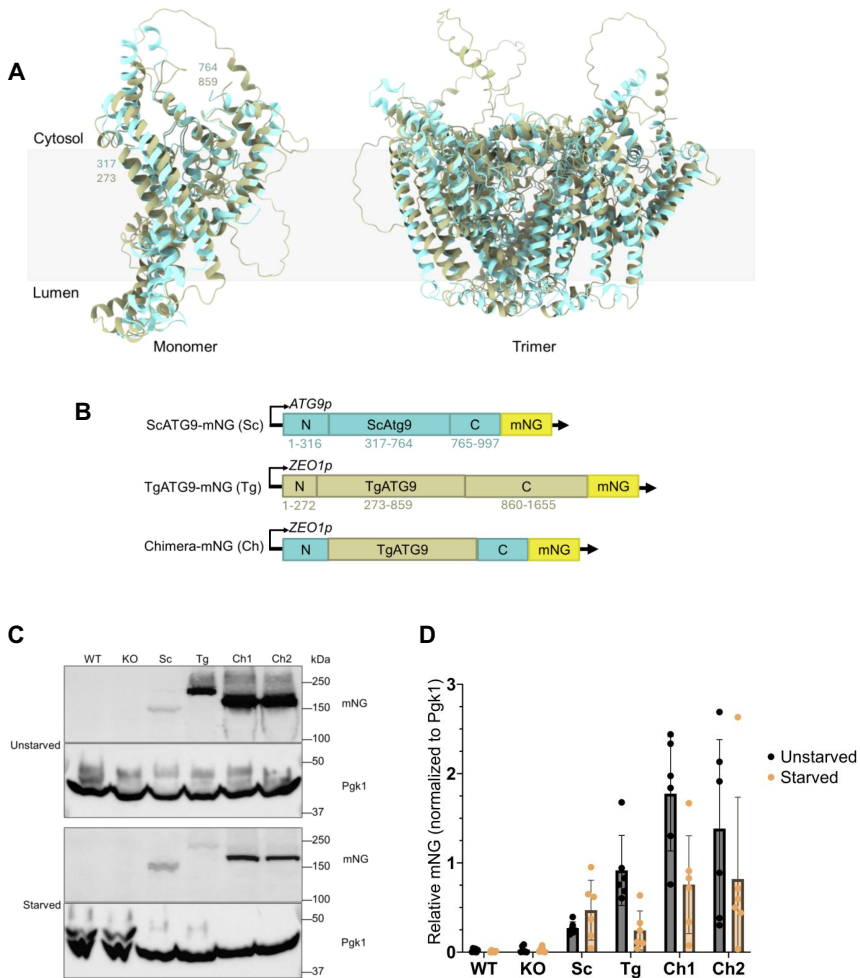


**Figure 1.** TgATG9 structural alignment with ScAtg9 and generation of constructs used for complementation assays. (A) Structural alignment of the AlphaFold3 predicted “core” structures of TgATG9 (olive) and ScAtg9 (cyan) using ChimeraX with a lipid bilayer depicted to represent orientation within a membrane. Both monomeric and trimeric forms are shown. (B) Plasmids containing constructs used for yeast complementation. The yeast *ATG9* promoter (*ATG9p*) was used to drive expression of ScAtg9 while the strong, constitutive *ZEO1* promoter (*ZEO1p*) was used to drive expression of constructs containing TgATG9 sequences. All constructs had mNeonGreen (mNG) appended to the C terminus. Numbers denote amino acid position. ScAtg9-mNG is abbreviated as Sc, TgATG9-mNG is abbreviated as Tg, and the Chimera-mNG construct is abbreviated as Ch. (C) Western blot validation from total lysate of protein expression of constructs used for yeast complementation in unstarved and starved conditions (24 h nitrogen starvation). Uncomplemented wildtype (WT) and *atg9Δ* knockout (KO) yeast were included as untagged controls. Pgk1 was used as a loading control. Ch1 and Ch2 are two separate, genetically identical, isolates of the chimeric (Ch) construct. (D) Relative mNG signals quantified from (C) normalized to Pgk1 loading controls. Bars represent mean  $\pm$  SD ( $n=6$  biological replicates).

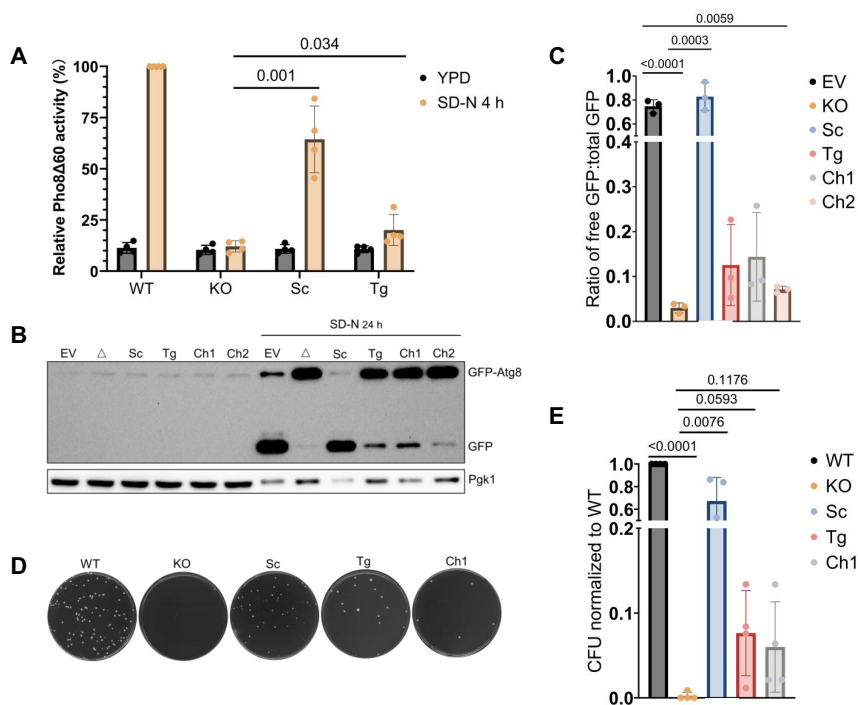


**Figure 2.** TgATG9 partially rescues bulk autophagy in *atg9Δ* knockout yeast. (A) Relative Pho8Δ60 activity normalized to wildtype (WT) controls for yeast *atg9Δ* (KO) and KO complemented with ScAtg9 (Sc) or TgATG9 (Tg) in nutrient-rich (YPD) or nitrogen-starvation (SD-N 4 h) conditions ( $n=4$  biological replicates). Bars represent mean  $\pm$  SD. Statistical analysis was done using a paired Student's *t*-test with p-values denoted above bars. (B, C) GFP-Atg8 processing assay. Representative western blot (B) depicting GFP-Atg8 or free GFP in unstarved or starved conditions (SD-N 24 h). WT control with empty vector (EV) or KO ( $\Delta$ ) were complemented with plasmids containing ScAtg9 (Sc), TgATG9 (Tg), or two independent isolates of the chimera (Ch1 and Ch2) constructs. Pgk1 was used as a loading control. (C) Ratio of free GFP:total GFP quantified from (B). Bars represent mean  $\pm$  SD. Statistical analysis was done using a one-way ANOVA with Tukey's multiple comparisons followed by an unpaired Student's *t*-test with p-values denoted above bars ( $n=3$  biological replicates). (D, E) CFU viability assay. Representative images from 100  $\mu$ L (1 OD diluted to  $10^{-4}$ ) plated cells after 6 days of nitrogen starvation then grown in YPD for 2 days. (E) Quantification of (D) normalized to WT controls. Bars represent mean  $\pm$  SD. Statistical analysis was done using a one-way ANOVA with Tukey's multiple comparisons followed by an unpaired Student's *t*-test with p-values denoted above bars ( $n=3$  biological replicates).

constructs containing *T. gondii* sequences (Tg and two independent isolates of the chimera, Ch1 and Ch2) were able to partially rescue the autophagy defect of *atg9Δ* cells (Figure 2B-C) [53]. Interestingly, there appeared to be no statistical differences between the level of rescue by TgATG9 or the two independent isolates of the chimera. All constructs with *T. gondii* sequences

were unable to fully restore autophagy to the same levels as the wild type or yeast complemented with ScAtg9. Finally, we examined yeast viability because loss of autophagy causes a loss of viability [54,55]. To determine the effects on yeast viability, cells were plated after 6 days starvation then grown on YPD for 2 days. Wild-type cells survived starvation of this duration (Figure 2D-E). In contrast, the majority of *atg9Δ* knockout yeast plates had no colony-forming units (CFUs) observed. For cells complemented with the ScAtg9, TgATG9 and Ch1 constructs, CFUs were quantified and normalized to the wild type, which reproduced the partial rescue phenotype seen by the Pho8Δ60 and GFP-Atg8 processing assays.

Additionally, while the main scramblase activity of Atg9 is conferred by its transmembrane region, the N- and C-termini contain phosphorylation sites necessary for Atg9 activity or stability [49,56]. We searched the *Toxoplasma* database (ToxoDB) and found that TgATG9 contains six phosphorylation sites based on published phosphoproteomics studies (Figure S2A-B) [57,58]. We generated TgATG9 phosphorylation mutant parasites (S165A, S933A, S1316A, S1332A, S1377A, S1482A) in a tdTomato-TgATG8-expressing *T. gondii* strain. We assessed autophagy function by using a fluorescent dye (CytolD) that stains autolysosomes, including those of *T. gondii* [15,25,59-62]. CytolD staining was performed after treatment with the cathepsin protease L (TgCPL) inhibitor LHVS to allow for autophagic material to accumulate for visualization [15,63]. Both wild-type (ME49) and TgATG9 phosphorylation mutant parasites accumulated CytolD-positive puncta after LHVS treatment, suggesting that TgATG9 phosphorylation status was not critical for autophagic function (Figure S2C-D).

Taken together, our data demonstrate that while TgATG9 is dissimilar in many ways to ScAtg9 including size and post-translational modifications, it contains a core transmembrane structure that likely confers phospholipid scramblase function, among other roles of Atg9/ATG9 proteins, that can partially rescue bulk autophagy in *atg9Δ* knockout yeast.

### **Conditional knockdown of TgATG9 disrupts bradyzoite autophagy**

We previously demonstrated the importance of TgATG9 in *T. gondii* autophagy using a parasite line harboring a stable TgATG9 genetic knockout. However, we could not rule out indirect effects or delayed effects from the complete absence of TgATG9 on bradyzoite biology [25]. To provide direct evidence that TgATG9 is critical and specific for autophagy, we generated a conditional knockdown mutant of TgATG9 using the auxin-inducible degron (AID) system that confers post-translational reversible regulation [64]. In parasites expressing the heterologous F-box protein TIR1, TgATG9 was endogenously tagged at the C terminus with a minimal auxin-inducible degron (mAID) fused to the mNeonGreen fluorophore (Figure 3A) [65]. Upon



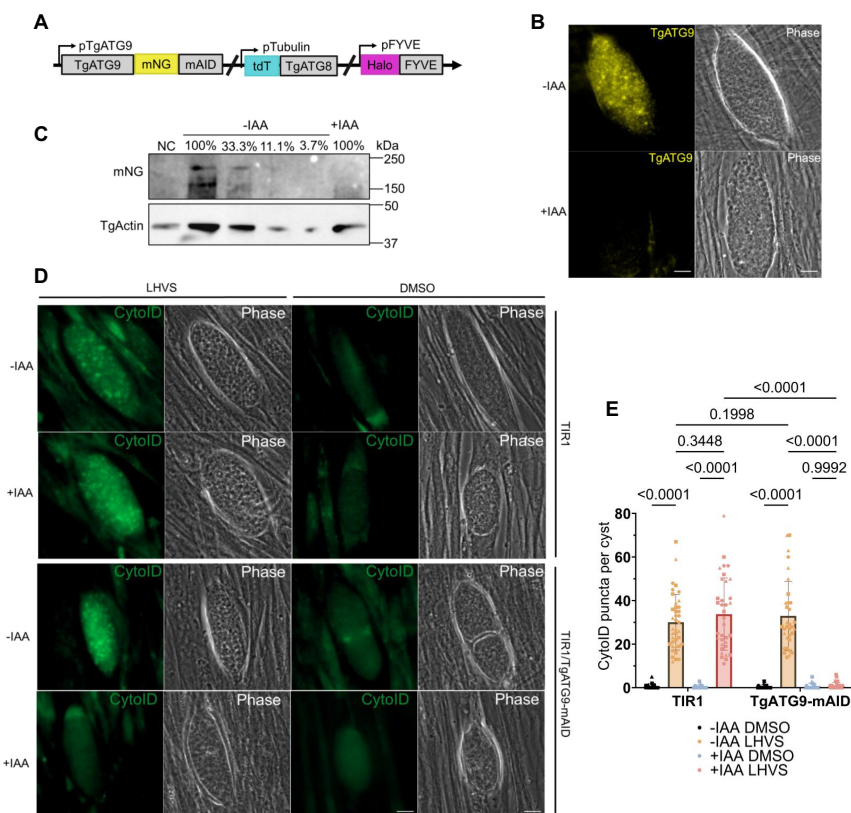


**Figure 3.** Conditional knockdown (KD) of TgATG9 disrupts bradyzoite autophagy. (A) Endogenous tagging of TgATG9 with mNeonGreen (mNG) and the minimal auxin inducible degron (mAID) was achieved with CRISPR-Cas9 and homology-directed repair. tdTomato (tdT)-TgATG8 was subsequently introduced as an exogenous copy by insertion into the tubulin locus. Endogenous tagging of TgFYVE with HaloTag (Halo) was subsequently achieved with CRISPR-Cas9 and homology-directed repair to generate triple-fluorescent parasites. (B) Fluorescent-imaging of *in vitro* TgATG9-mAID differentiated cysts treated with IAA or vehicle control for 24 h. Scale bars: 10  $\mu$ m. Representative images shown (n=3 biological replicates). (C) Western blot from total bradyzoite lysates of conditional KD of TgATG9-mAID with IAA or vehicle control for 24 h. Serial dilution of vehicle treated parasites were used for relative quantification of protein levels. TgActin was used as a loading control. (D) Autolysosome staining (CytolD) of *in vitro* TIR1 or TgATG9-mAID (TIR1/TgATG9-mAID) differentiated cysts treated with or without LHVS and IAA or vehicle control for 72 h. Scale bars: 10  $\mu$ m. (n=3 biological replicates, representative images shown). (E) Quantification of (D) as number of CytolD puncta per cyst. Each point represents a single cyst with different shapes corresponding to each biological replicate. Bars represent mean  $\pm$  SD. Statistical analysis was done using ordinary two-way ANOVA with Tukey's multiple comparisons with p-values denoted above bars (n=3 biological replicates,  $\geq 10$  cysts quantified per replicate).



addition of auxin (indole-3-acetic acid, IAA), we observed efficient conditional knockdown of TgATG9-mAID in *in vitro* bradyzoites after 24 h by live fluorescence microscopy and western blotting (Figure 3B-C). Next, we assessed the impact of conditional knockdown of TgATG9-mAID on bradyzoite autophagy by differentiating *in vitro* bradyzoites for 7 days followed by treatment with IAA or vehicle control with or without LHSV for 3 days prior to CytolD staining. Bradyzoites of the TIR1 parental strain accumulated CytolD-positive autolysosomes in the presence or absence of IAA treatment, as expected (Figure 3D). Similarly, without IAA treatment TgATG9-mAID parasites accumulated CytolD-positive autolysosomes. However, TgATG9-mAID bradyzoites treated with IAA showed markedly reduced CytolD-positive staining of autolysosomes (Figure 3D-E). These findings provide direct evidence that TgATG9 is important for bradyzoite autophagy and establish a conditional knockdown system to allow us to assess the direct impacts of acute disruptions to this pathway.

### ***TgATG9 is required for autophagosome biogenesis and proper autophagic flux***

To define the role of TgATG9 in autophagic flux, we first confirmed the subcellular localization of TgATG9 within bradyzoites by performing immunofluorescence staining and quantified colocalization to known autophagy markers in fixed samples. TgATG9 colocalized with TgCPL (PLVAC marker) and TgATG8 (Figure S3). We included staining for ATRX1, an apicoplast marker, as a control and showed that TgATG9 colocalizes more significantly to autophagic structures rather than the apicoplast, in agreement with previous studies performed in tachyzoites [24]. While these data provide insight into the location of TgATG9 within bradyzoites, we recognize that they are only two-dimensional snapshots of an intrinsically dynamic process. Therefore, we wanted to assess the dynamics of this pathway by live microscopy.

We hypothesized that the acute disruption of bradyzoite autophagy would result in altered dynamics between TgATG9, TgATG8, and the PLVAC. Using our TgATG9-mAID strain, which also has mNeonGreen fused to TgATG9, we further generated a triple-fluorescent parasite strain by ectopically expressing tdTomato-TgATG8 as a marker of autophagosomes and endogenously HaloTag-tagging TgFYVE as a marker for the PLVAC (Figure 3A) [66,67]. Given that there are many bradyzoites tightly packed and randomly oriented within an intracellular cyst, we aimed to capture autophagosome dynamics in a 3-dimensional manner over a time course of several minutes utilizing lattice light sheet microscopy (LLSM) to image live, *in vitro* differentiated cysts. LLSM permits rapid imaging of several planes over a given time course and therefore is well suited to capture cellular dynamics within the 3-dimensional structure of cysts with minimal photobleaching [68-70].

Using our triple-fluorescent parasites, we assessed the direct effects of conditional knockdown of TgATG9-mAID by LLSM (Figure 4A). Parasites were differentiated into bradyzoites *in vitro* for 7 days prior to treatment with IAA or vehicle control for 24 h. We then imaged intracellular cysts containing bradyzoites over the course of 5 min. First, we observed a reduction in TgATG9 puncta in the IAA-treated cysts, validating the effectiveness of our conditional knockdown (Figure 4B, Video S1). Within untreated cysts, we observed examples of the spatiotemporal dynamic associations between TgATG9, TgATG8, and the PLVAC resembling autophagosome trafficking to the digestive organelle or autophagosome fusion

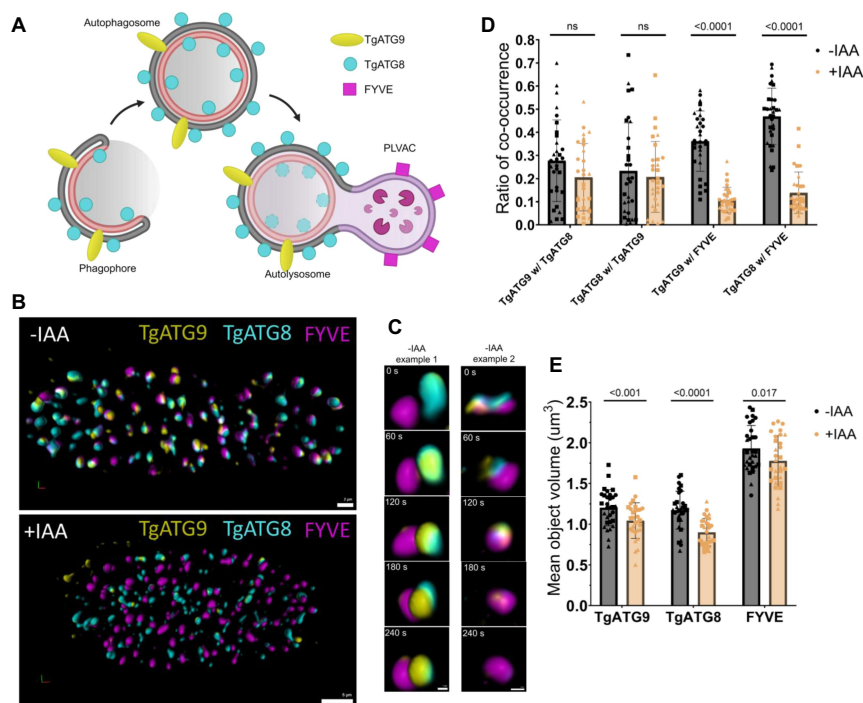


**Figure 4.** Conditional KD of TgATG9 disrupts dynamic associations between autophagosomes and the PLVAC in bradyzoites. (A) Schematic of fluorescent markers monitored in lattice light sheet microscopy (LLSM) experiments created with BioRender. (B) Representative *in vitro* differentiated cysts imaged with LLSM treated with IAA or vehicle control for 24 h. Scale bars: 2  $\mu$ m (top) and 5  $\mu$ m (bottom). (C) Representative examples of dynamic associations between TgATG9, TgATG8, and FYVE imaged with LLSM in untreated parasites (-IAA). Scale bars: 1  $\mu$ m (left) and 5  $\mu$ m (right). Volumetric renderings for (B, C) generated with Arivis Vision4D software. (D, E) Quantification of the ratio of co-occurrence and mean object volumes among TgATG9, TgATG8, and TgFYVE from LLSM. Bars represent mean  $\pm$  SD. Statistical analysis was done using paired Student's *t*-test with p-values denoted above bars. (n= 3 biological replicates,  $\geq 10$  cysts' total volumes were imaged per treatment condition over 5 min per replicate).

with the PLVAC (Figure 4C, Video S2). We quantified the degree of colocalization between the various markers, accounting for the knockdown of TgATG9, reported as a ratio of co-occurrence. Globally, on a per cyst level, IAA-treated bradyzoites displayed a significant reduction in the co-occurrence of TgATG9 or TgATG8 with the PLVAC, suggesting decreased autophagic flux due to impaired delivery of autophagosomes to the PLVAC compared to vehicle-treated controls (Figure 4D); there was essentially no difference in the co-occurrence between TgATG9 and TgATG8. Using Arivis Vision4D software, we generated volumetric renderings of the three markers and calculated their mean object volumes within a given cyst. IAA-treated parasites had significantly smaller TgATG9 and TgATG8 puncta compared to vehicle-treated controls, indicating an impairment in the biogenesis and enlargement of autophagosomes (Figure 4E). Additionally, TgATG9 knockdown bradyzoites had significantly smaller PLVACs, which is consistent with decreased delivery of autophagic material to the PLVAC.

Thus, our findings support the direct role of TgATG9 in autophagosome biogenesis in bradyzoites whereby acute disruption of the autophagy pathway results in decreased autophagic flux through altered dynamics between autophagosomes and delivery of autophagic material to the PLVAC.

### ***Bradyzoite autophagy is required for maintenance of chronic infection in vitro***

While we have demonstrated that bradyzoites with a stable genetic knock-out of *TgATG9* have reduced viability, we cannot rule out any accumulated effects from the absence of TgATG9 in establishment or persistence of chronic infection [25]. Although TgATG9 is not essential for normal tachyzoite growth, TgATG9 knockout tachyzoites have reduced viability after extracellular stress and have decreased virulence during mouse infection [24]. To pinpoint the role of TgATG9 and autophagy in parasite persistence specifically within the bradyzoite stage, we assessed bradyzoite viability after conditional knockdown of TgATG9 post-differentiation *in vitro*. TIR1 or TgATG9-mAID parasites were differentiated into bradyzoites for 7 days then treated with constant IAA or vehicle control for an additional 7 days with daily media changes. After the 7 days of treatments, bradyzoites were harvested from cultured cysts using pepsin and their viability was assessed by plaque assay with qPCR normalization of parasite genomes (Figure 5A) [71]. IAA treatment had no effect on the viability of TIR1 bradyzoites, while IAA-treated TgATG9-mAID parasites had significantly reduced viability (Figure 5B). Our results emphasize the importance of TgATG9 and autophagy in sustaining bradyzoite survival and clarify their critical role in the maintenance of chronic infection *in vitro*.

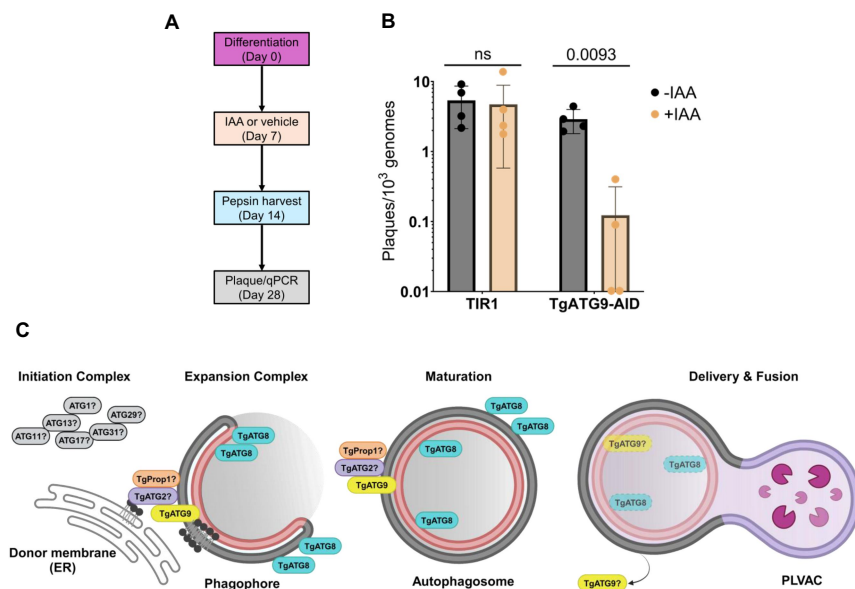


**Figure 5.** *T. gondii* bradyzoite autophagy is required for maintenance of chronic infection *in vitro*. (A) Schematic of bradyzoite viability assay. Parasites were differentiated in alkaline-stress media for 7 days prior to initiation of treatment with IAA or vehicle control for another 7 days with daily media changes. Bradyzoites were harvested after 7 days treatment (Day 14) via pepsin harvest and directly used for plaque assay and genomic DNA extraction for qPCR. Plaques were quantified after 14 days (Day 28). (B) Viability of *in vitro* 7-days differentiated bradyzoites after 7 days treatment with IAA or vehicle control reported as number of plaques normalized to number of parasite genomes. Bars represent mean  $\pm$  SD. Statistical analysis was done using paired Student's *t*-test with *p*-values denoted above bars. (*n* = 4 biological replicates). (C) Proposed model of the role of TgATG9 in autophagosome biogenesis in *T. gondii* canonical autophagy. Autophagy is initiated through complex signals including response to cellular stress or nutrient deprivation that thereby activates an initiation complex comprised of key proteins yet to be discovered and characterized in this system. Downstream of the initiation complex, TgATG9 is the only known transmembrane autophagy protein that resides on the developing phagophore that likely nucleates a putative membrane expansion complex with potential interactions with other key proteins involved in this process (putative TgATG2 and TgATG18/TgProp1 have yet to be discovered or characterized in this context). Lipids from a donor membrane such as the ER are transferred onto the phagophore for membrane expansion whereby TgATG9 may function to equilibrate donated lipids on the phagophore membrane, among other roles. TgATG8 also gets lipidated onto the autophagosome membrane during maturation. The mature autophagosome gets delivered to the parasite's digestive organelle (PLVAC) and fuses with the PLVAC for delivery of autophagic cargo that will undergo degradative and recycling processes within the PLVAC lumen. It remains unknown whether TgATG9 gets degraded within the PLVAC or whether *T. gondii* autophagy possesses a mechanism for the cycling of TgATG9 like other model systems. Schematic created with BioRender.

## Discussion

While it has been established that autophagy is critical for *T. gondii* bradyzoites, the early steps of the pathway remain poorly characterized. Here, we expand our understanding of an important component of this pathway, TgATG9, by providing additional evidence for its role in autophagosome biogenesis. We propose that TgATG9 contributes to the expansion of the phagophore and is important for proper autophagosome delivery to the PLVAC (Figure 5C). Although it is a much larger protein than ScAtg9 and has limited homology apart from the core domain, TgATG9 was able to partially rescue bulk autophagy in *atg9Δ* knockout yeast, which we validated across three independent complementation assays. We investigated the spatiotemporal dynamics of TgATG9 in bradyzoite autophagy through LLSM, finding that TgATG9 is key to proper autophagosome formation and delivery to the PLVAC. TgATG9 likely requires collaboration with other TgATGs that participate in the membrane expansion complex such as a lipid transfer protein (a hypothetical TgATG2) and phosphatidylinositol-3-phosphate/PtdIns3P-binding protein (TgProp1, an Atg18 ortholog). Whether *T. gondii* forms such a membrane expansion complex will require the discovery and further characterization of candidate proteins. The fate of TgATG9 upon autophagosome fusion with the PLVAC also remains elusive. TgATG9 may be degraded within the PLVAC or potentially cycled through unknown mechanisms. Additionally, the absence of known initiators or regulators of *T. gondii* autophagy further contributes to our incomplete understanding of this pathway.

Our yeast complementation studies demonstrated that expression of either full-length TgATG9 or a chimera of TgATG9/ScAtg9 resulted in partial rescue of bulk autophagy. There are several possible explanations for the lack of full rescue. We determined the boundaries for the “core” region of TgATG9 and ScAtg9 based on a protein-protein BLAST search which may not have accurately mapped the true “core” region of transmembrane domains and important flanking residues [72]. Atg9/ATG9 proteins are known to form homotrimers with each protomer’s transmembrane domains contributing to formation of a central cavity for scrambling lipids, a function that can be disrupted if interactions within the homotrimeric interface are altered [26,27,30,73]. Since we did not directly assess scramblase activity of TgATG9 in our experiments, additional studies are needed to definitively conclude that TgATG9 is indeed a lipid scramblase important in autophagosome biogenesis. In yeast, Atg9 is post-translationally modified through phosphorylation in Atg1-dependent and -independent manners. Such modifications regulate the cycling of Atg9 to phagophore assembly sites or protein levels of Atg9, thus controlling rates of autophagosome formation [49,56,74]. We considered the importance of these post-translational modifications when

designing the chimera, thereby preserving phosphorylated residues. However, we found that preservation of these sites did not improve the partial rescue phenotype observed compared to yeast complemented with the full-length TgATG9. We tested the importance of TgATG9 phosphorylation in *T. gondii* and found that the annotated phosphorylation sites are not important in bradyzoite autophagy. However, these sites are based on phosphoproteomic data from tachyzoites; hence, additional studies are needed to determine the extent of TgATG9 phosphorylation specifically in bradyzoites [58]. Nonetheless, our assessment of TgATG9 phosphorylation provides some insights into potential key differences in how autophagy may be regulated in *T. gondii*. This is particularly intriguing because an initiating kinase such as Atg1 or ULK1 has not been discovered in *T. gondii* [18,19]. Although our studies primarily focused on regions of TgATG9 and ScAtg9 with shared homology, consideration of dissimilar regions may uncover novel features which could expand our understanding of the evolution of autophagy among eukaryotes. Furthermore, we cannot rule out other potential functions of TgATG9 in addition to its role in autophagy. Additional studies are required to determine whether membrane associated with TgATG9 is also important to seed phagophore formation in *T. gondii* or as an organizational hub for proper autophagy progression [39-41].

We localized TgATG9 to autophagic structures marked with TgATG8 (autophagosomes) and TgFYVE (PLVAC) within bradyzoites and utilized LLSM to visualize these dynamic associations that became disrupted upon conditional knockdown of TgATG9. The decreased size of autophagosomes (TgATG9 and TgATG8) along with decreased colocalization between autophagosomes and the PLVAC indicate that TgATG9 is crucial for autophagosome biogenesis. Under normal conditions, we observed examples of autophagosome delivery or fusion with the PLVAC occurring within a few minutes, consistent with recently reported spatiotemporal observations of autophagosome formation [75]. However, our LLSM studies lacked single-cell resolution and to definitively determine or quantify the autophagosome dynamics within a single bradyzoite would require additional labeling of markers at the parasite membrane or inner membrane complex. Despite this, we provide the first spatiotemporal characterization of autophagosome biogenesis in *T. gondii* and demonstrate the feasibility of monitoring live subcellular dynamics in bradyzoites.

We assessed the role of parasite autophagy in maintenance of chronic infection *in vitro* and showed that conditional knockdown of TgATG9 post-differentiation results in reduced autophagy and bradyzoite viability. These findings suggest that TgATG9 and its role in autophagy is specifically important for bradyzoite survival after chronic infection is already established. This study therefore addresses any potential confounders of altered bradyzoite biology that were observed with the stable TgATG9 genetic knockout

including altered mitochondrial morphology, a phenotype observed as early as 6 days into *in vitro* differentiation. *TgATG9* knockout bradyzoites also display impaired replication and division along with a disorganized inner membrane complex [25]. While we did not directly investigate these changes with our conditional knockdown of *TgATG9*, we can infer that such changes did not come into play during the establishment of chronic infection in our experiments. Future studies could extend our *in vitro* findings into an *in vivo* mouse model to provide proof of concept that bradyzoite autophagy is selectively targetable to potentially curb chronic infection. We attempted to knockdown expression of *TgATG9-AID* in chronically infected mice, but the results were inconclusive because we could not quantify the extent of knockdown and brain exposure of IAA and other analogs is limited [76]. Expression of *TgATG9* from a tachyzoite specific promoter might be effective but we have found that this approach doesn't work in every case. [15,77,78]. Furthermore, the mechanism by which bradyzoites are dying remains to be elucidated. Additional studies are required to determine how disrupting autophagy affects bradyzoite biology, perhaps due to accumulation of damaged organelles, altered metabolism, or activated cellular death pathways. Our *TgATG9* conditional knockdown mutant can be used in future metabolomic or proteomic studies for this purpose, which may also reveal effects of *TgATG9* depletion unrelated to its function in the *T. gondii* autophagy pathway. While several other pathways have been reported to be critical to bradyzoite survival including storage and utilization of amylopectin granules, maintaining structural integrity of the cyst wall, and apicoplast-related functions, our results underscore the importance of autophagy in this stage of *T. gondii* [8,79-82].

Taken together, our study advanced understanding of the contributions from *TgATG9* to autophagosome biogenesis in bradyzoites and maintenance of chronic infection. Further characterization of the autophagy pathway, particularly the poorly understood early steps, will provide valuable insights into the evolution, mechanism, and regulation of this indispensable process that can be strategically manipulated to target chronic infection.

## Materials and methods

### *Structural prediction and alignment of TgATG9 and ScAtg9*

A predicted structure of the *TgATG9* (TGME49\_260640) monomer was generated using AlphaFold3 implemented in the AlphaFold server platform (<https://alphafoldserver.com/>) [46]. The "core" sequence of *TgATG9* (273-859) was used as the search input. Five predicted models were generated and ranked based on pLDDT and PAE scores. The top-ranked model of *TgATG9* (273-859) was structurally aligned with the "core" region of



a monomer or trimer of the AlphaFold3 predicted model of *Saccharomyces cerevisiae* Atg9 using Matchmaker structure analysis in UCSF ChimeraX version 1.7.1 [83]. A figure of the aligned predicted structures was prepared in ChimeraX.

### ***Yeast strains, media, and growth conditions***

All yeast *Saccharomyces cerevisiae* strains used in this study are listed in Table S1 [56,84-86]. Gene deletions and chromosomal tagging were performed using standard methods [87]. Yeast cells were cultured at 30°C in rich medium (YPD; 1% yeast extract [Formedium, YEA04], 2% peptone and 2% glucose) as nutrient-rich conditions. To induce autophagy, cells in mid-log phase (OD<sub>600</sub> = 0.4-0.8) were shifted from YPD to nitrogen starvation medium (SD-N; 0.17% yeast nitrogen base without ammonium sulfate or amino acids [Formedium, CYN0501], containing 2% glucose) for the indicated times.

### ***Generation of plasmids for yeast complementation***

To generate the plasmids for the yeast autophagy complementation experiments, plasmid pRS406-ATG9p-ScAtg9-mNeonGreen was constructed by amplifying the *ATG9* promoter region (−1000-0) and *ATG9* ORF by PCR from genomic DNA. The PCR product was inserted into the pRS406-mNeonGreen plasmid using Gibson Assembly. Of note, the *ZEO1* promoter region (−550-0) was amplified by PCR from genomic DNA and then the PCR product was used to replace the *ATG9* promoter region on the pRS406-ATG9p-ScAtg9-mNeonGreen plasmid by Gibson Assembly to construct the pRS406-ZEO1p-ScAtg9-mNeonGreen plasmid to facilitate other plasmid construction. Plasmid pRS406-ZEO1p-TgAtg9-mNeonGreen plasmid was constructed by replacing the *ATG9* ORF region on the pRS406-ZEO1p-ScAtg9-mNeonGreen plasmid with the *TgATG9* ORF region amplified from genomic DNA. Similarly, plasmid pRS406-ZEO1p-Sc/TgAtg9chimera-mNeonGreen plasmid was constructed by replacing the “core” *ATG9* ORF of ScAtg9 region on the pRS406-ZEO1p-ScAtg9-mNeonGreen plasmid with the “core” *TgATG9* ORF region amplified from genomic DNA. Before transformation, pRS406-based plasmids were cut with BstBI at 65°C.

### ***Yeast complementation assays***

#### ***Pho8Δ60 assay***

Pho8Δ60 assays were performed as previously described [52].

### ***GFP-Atg8 processing assay***

GFP-Atg8 processing assays were performed as previously described [88]. Rabbit anti-Pgk1 antiserum is a generous gift from Dr. Jeremy Thorner (University of California, Berkeley; 1:1000). Other antibodies were from the following sources: mouse anti-YFP, which detects GFP in our study (Clontech, 63281; 1:5000), goat anti-rabbit IgG secondary antibody (Fisher, ICN55676; 1:10000) and rabbit anti-mouse IgG secondary antibody (Jackson, 315-035-003; 1:10000). The blot was imaged using ChemiDoc Touch imaging system (Bio-Rad, 1708370) and quantified using Bio-Rad Image Lab software.

### ***CFU viability assay***

Yeast cells were grown in YPD to mid-log phase and then shifted to SD-N medium for nitrogen starvation. After 6 days starvation, 1 OD<sub>600</sub> units of cells were collected, resuspended in 1 mL of SD-N medium (1 OD<sub>600</sub>/mL) and then subjected to serial dilution. 100  $\mu$ L of  $10^{-4}$  diluted samples were spread onto YPD plates and incubated at 30°C for 2 days before imaging.

### ***Parasite and host cell culture***

All *T. gondii* parasites were cultured in human foreskin fibroblasts (HFFs, Hs27) obtained from the American Type Culture Collection (ATCC-CRL-1634). Tachyzoite growth was maintained at 37°C under 5% CO<sub>2</sub> in D10 medium, comprising DMEM (Fisher Scientific, 10-013 cv), 10% heat-inactivated bovine calf serum (Cytiva, SH30087.03), 2 mm L-glutamine (Corning, 25-005-CI), and 50 U/mL of penicillin-streptomycin (Gibco, 15070063). For all bradyzoite differentiation, tachyzoites were mechanically lysed from infected HFF monolayers via scraping and syringing (20- and 25-gauge needles) and allowed to invade fresh monolayers of HFFs for 24 h at 37°C under 5% CO<sub>2</sub> in D10 medium. The following day, D10 medium was replaced with alkaline-stress medium consisting of RPMI-1640 without NaHCO<sub>3</sub> (Cytiva, SH30011.02) supplemented with 3% heat-inactivated fetal bovine serum (Cytiva, SH30396.03), 50 mm HEPES (Sigma-Aldrich, H3375), 50 U/mL of penicillin-streptomycin and adjusted to pH 8.2-8.3 with NaOH. All bradyzoites were cultured at 37°C under ambient CO<sub>2</sub> conditions with daily medium changes to ensure alkaline pH [89].

### ***T. gondii transfection***

Intracellular tachyzoites were mechanically lysed from infected HFF monolayers via scraping and syringing (20- and 25-gauge needles). Parasites were pelleted and resuspended in cytomix transfection buffer (2 mm EDTA, 120 mm KCl, 0.15 mm CaCl<sub>2</sub>, 10 mm K<sub>2</sub>HPO<sub>4</sub>/KH<sub>2</sub>PO<sub>4</sub>, 25 mm HEPES, 5 mm MgCl<sub>2</sub>, pH 7.6). For each transfection, guide RNA plasmids, homology-direct

repair templates, or linearized plasmids were precipitated with ethanol and resuspended in cytomix transfection buffer. The DNA mixture was combined with pelleted parasites followed by electroporation in 0.4-cm cuvettes (Bio-Rad, 1652081), utilizing GenePulser Xcell with PC and CE modules (Bio-Rad, 1652660), and configured with the following parameters: 2400 V voltage, 25  $\mu$ F capacitance, 50  $\Omega$  resistance.

### **T. gondii strain generation**

Primers and oligos were synthesized either by IDT or Sigma-Aldrich. All guide RNAs were generated by substituting the original 20 base pair guide RNA sequence on the plasmid pCas9/sgRNA/Bleo [90] with desired 20 base pair guide RNA sequence, using the Q5<sup>®</sup> Site-Directed Mutagenesis Kit (New England Biolabs, E0554S). Homology-directed repair templates were PCR amplified using the CloneAmp<sup>™</sup> HiFi PCR Premix (Takara Bio, 639298). Guide RNA and repair template sequences are listed in Table S1.

### **Generation of the TgATG9-mAID *T. gondii* strain**

Starting with the TIR1-expressing ME49 *T. gondii* strain (ME49/TIR1) [65], TgATG9 was endogenously tagged at the C terminus to generate ME49/TIR1/TgATG9-mAID (TgATG9-mAID) parasites. A guide RNA targeting the C terminus of TgATG9 near the stop codon was generated using oligos P1/P2. Homology-directed repair template was generated using oligos P3/P4 for PCR amplification of pGL015 [91] containing the Xten linker, V5 epitope (Invitrogen, 37-7500), mNeonGreen, minimal AID, and Ty epitope. ME49/TIR1 parasites were co-transfected with 100  $\mu$ g guide RNA and 50  $\mu$ g repair template. At 48 h after transfection, positively transfected parasites were selected using 5  $\mu$ g/mL phleomycin (Invitrogen, NC9198593) prior to isolating clones by limiting dilution. Individual parasite clones were validated by PCR amplification to confirm presence of the mAID tag using P5/P6 and live imaging for mNeonGreen fluorescence.

### **Generation of the triple-fluorescent *T. gondii* strain used in LLSM**

Starting with the ME49/TIR1/TgATG9-mAID (TgATG9-mAID) *T. gondii* strain, a triple-fluorescent strain was generated by ectopic expression of tdTomato-TgATG8 and endogenous tagging of HaloTag-TgFYVE at the N-terminus. Plasmids containing pTubulin-tdTomato-TgATG8-BLE [15] were linearized with PmeI and 100  $\mu$ g was transfected into TgATG9-mAID parasites for single crossover integration into the tubulin locus. tdTomato<sup>+</sup> parasites were enriched by sorting 48 h post-transfection prior to isolating clones by limiting dilution and phleomycin selection. Individual parasite clones (ME49/TIR1/

TgATG9-mAID/tdTomato-TgATG8) were validated by live imaging for tdTomato fluorescence. In parallel, the parental ME49/TIR1 *T. gondii* strain was also co-transfected with the same amount of linearized plasmids to generate ME49/TIR1/tdTomato-TgATG8 parasites to be used as controls in LLSM.

Subsequently, a homology-directed repair template was generated using oligos P7/P8 for PCR amplification of a FLAG-HaloTag-containing plasmid (phage-ubc-flag-halo-baCDS-baUTR1-24xMS2V5-wpre, Louis M. Weiss lab [Albert Einstein College of Medicine] unpublished). Double-fluorescent (ME49/TIR1/TgATG9-mAID/tdTomato-TgATG8) parasites were co-transfected with 100 µg of a guide RNA targeting the N terminus of TgFYVE (TGME49\_237870) [67] and 50 µg repair template. At 48 h after transfection, positively transfected parasites were selected using 5 µg/mL phleomycin prior to isolating clones by limiting dilution. Individual parasite clones (ME49/TIR1/TgATG9-mAID/tdTomato-TgATG8/HaloTag-FYVE) were validated by PCR amplification to confirm presence of the HaloTag using P9/P10. In parallel, the ME49/TIR1/tdTomato-TgATG8 *T. gondii* strain was also co-transfected with the same amounts of guide RNA and repair template to generate ME49/TIR1/tdTomato-TgATG8/HaloTag-FYVE parasites to be used as controls in LLSM.

### **Widefield fluorescence microscopy**

For live microscopy used to validate conditional knockdown of TgATG9-mAID, parasites were differentiated into bradyzoites for 7 days in 35-mm dish, No. 1.5 coverslip, 14-mm diameter, tissue culture dishes (MatTek, P35G-1.5-14-C) in phenol red free alkaline-stress medium consisting of modified RPMI-1640 without phenol red or NaHCO<sub>3</sub> (Sigma-Aldrich, R8755) supplemented with 3% heat-inactivated fetal bovine serum, 50 mM HEPES, 50 U/mL of penicillin-streptomycin and adjusted to pH 8.2-8.3 with NaOH. After 7 days differentiation, bradyzoites were treated with 500 µM IAA (Sigma-Aldrich, I2886) or an equal volume ethanol vehicle control for 24 h for conditional knockdown of TgATG9-mAID. Widefield microscopy images were taken on a Zeiss Axio Observer Z1 inverted microscope at 40× and analyzed using Zen 3.7 blue edition software. For imaging of fixed samples for all CytolD experiments, images were taken at 63× and analyzed using Zen 3.7 blue edition software.

### **Immunoblotting**

For validation of TgATG9 knockdown by immunoblot, TgATG9-mAID parasites were differentiated into bradyzoites for 7 days grown in alkaline-stress medium (ambient CO<sub>2</sub>) with daily media changes. On day 7, bradyzoites were

treated with 500  $\mu\text{M}$  IAA (Sigma-Aldrich, I2886) or ethanol vehicle control for 24 h. Bradyzoites were harvested via scraping, syringing (20- and 25-gauge needles), pepsin treatment (0.026% pepsin [Sigma-Aldrich, P7000] in 170 mM NaCl and 60 mM HCl, final concentration), and filtration. Bradyzoites were enumerated and lysed with RIPA buffer (Thermo Scientific, 89900) supplemented with cOmplete Mini Protease Inhibitors cocktail (Roche, 11836153001) for 15 min on ice with gentle rocking. Lysates were centrifuged at 4°C for 10 min at 20,000  $\times g$ . Lysates were supplemented with 5X SDS-PAGE sample buffer and 10%  $\beta$ -mercaptoethanol, resulting in a final concentration of 1X SDS-PAGE buffer and 2%  $\beta$ -mercaptoethanol. The final concentration was  $\sim 4 \times 10^7$  bradyzoites per 25  $\mu\text{L}$  and designated as 100% for loading.

Lysates were subjected to SDS-PAGE using a gradient 4-12% NuPAGE™ Bis-Tris gel (Invitrogen, NP0321) and transferred onto 0.45- $\mu\text{m}$  nitrocellulose membranes (Bio-Rad, 1620115) with Trans-Blot® SD semi-dry transfer cell (Bio-Rad, 1703940) for 45 min at 18 V at room temperature. Following transfer, membranes were blocked with 5% milk in phosphate-buffered saline (PBS [Gibco, 21600010])-T (PBS with 0.05% Triton X-114 [Sigma-Aldrich, X114] and 0.05% Tween-20 [Fisher Scientific, 170-6531]) for 30 min at room temperature. Primary antibodies were diluted in 1% milk in PBS-T and applied to membranes overnight at 4°C. Primary antibodies used include mouse anti-mNeonGreen (Chromotek, 32F6; 1:1000), rabbit anti-TgActin (Sibley lab, Washington University in St. Louis; 1:20,000). After primary antibody incubation, membranes were washed 3 times with PBS-T before incubation with HRP-conjugated secondary antibodies (Jackson ImmunoResearch Laboratories, 115-035-146; 1:5000) for 1 h at room temperature. Proteins were detected using SuperSignal™ West Pico PLUS Chemiluminescent Substrate or Femto Maximum Sensitivity Substrate (Thermo Fisher, 1863096 or 34095). The Syngene PXi6 imaging system with Genesys (v1.8.2.0) software was used to detect signals, and Fiji (v2.9.0/1.53t) [92] was used for quantification.

### **CytoID staining of autolysosomes**

*T. gondii* tachyzoites were differentiated into bradyzoites in 6-well tissue culture plates with 22 mm  $\times$  22 mm No. 1.5 coverslips (Globe Scientific, 1404-15) for 7 days then treated with 1  $\mu\text{M}$  LHSV (Sigma-Aldrich, SML2857) or equal volume DMSO for 3 days. For knockdown of TgATG9-mAID, bradyzoites were also concurrently treated with 500  $\mu\text{M}$  IAA or equal volume ethanol for 3 days. The CytoID Autophagy Detection Kit 2.0 (Enzo, ENZ-KIT175) was used to stain autolysosomes within live bradyzoites for 45 min prior to fixation with 4% paraformaldehyde, following the manufacturer's instructions. Fixed coverslips were mounted using ProLong™ Gold Antifade Mountant (Thermo Scientific, P36930). Images were taken on a Zeiss Axio

Observer Z1 inverted microscope at 63× and analyzed using Zen 3.7 blue edition software. For quantification of the number of CytolD puncta within each cyst, CytolD-positive puncta were enumerated from at least 10 cysts per biological replicate, from 3 biological replicates total. All images were coded prior to quantification to blind the experimenter during quantification.

### **Live cell lattice light sheet microscopy (LLSM)**

ME49/TIR1, ME49/TIR1/tdTomato-TgATG8/HaloTag-FYVE, and triple-fluorescent (ME49/TIR1/TgATG9-mAID/tdTomato-TgATG8/HaloTag-FYVE) *T. gondii* strains were differentiated into bradyzoites for 7 days in 35-mm dish, No. 1.5 coverslip, 14-mm diameter, tissue culture dishes (MatTek, P35G-1.5-14-C) in phenol red free alkaline-stress medium consisting of modified RPMI-1640 without phenol red or NaHCO<sub>3</sub> (Sigma-Aldrich, R8755) supplemented with 3% heat-inactivated fetal bovine serum, 50 mM HEPES, 50 U/mL of penicillin-streptomycin and adjusted to pH 8.2-8.3 with NaOH. After 7 days differentiation, bradyzoites were treated with 500 μM IAA or an equal volume of ethanol as a vehicle control for 24 h for conditional knockdown of TgATG9-mAID. Prior to live cell imaging, bradyzoites were incubated with phenol red free alkaline-stress medium containing 200 nM Janelia Fluor® HaloTag® 646 ligand (Promega, GA1120) for 15 min to label HaloTag-FYVE. After the incubation period, fresh phenol red free alkaline-stress medium was added.

Live imaging of *in vitro* *T. gondii* cysts was performed using a ZEISS (Carl Zeiss Inc., Oberkochen, Germany) lattice lightsheet 7 microscope (44.83X/1.0 NA Objective at 60° angle to the cover glass, Pco.edge 4.2 CLHS sCMOS camera). The whole cyst volume was imaged in 20s for a total duration of 5 min with an acquisition of 15 ms exposure for 488 nm, 561 nm, and 640 nm excitations at individual imaging depth. Collected volumes were cropped in Zen 3.5 (Carl Zeiss Inc., Oberkochen, Germany). Images were deconvolved using Zen's built in deconvolution tool. The deconvolved images were then deskewed in Zen to transform the skewed images into an orthogonal coordinate system based on the coverslip geometry.

### **Quantification of lattice light sheet microscopy (LLSM)**

Deconvolved and deskewed volumes were imported into Arivis Vision4D 4.0 (Carl Zeiss Inc., Oberkochen, Germany). A linear rotation was applied to each volume and the volumes were further cropped to reduce the data size prior to preprocessing.

Determination of background fluorescence was calculated. Due to inherent parasite autofluorescence and slight bleed through from tdTomato into the 488-nm channel, we used data captured from the non-mNeonGreen-expressing cysts to control for this and to more accurately distinguish true

mNeonGreen signal in strains expressing TgATG9-mAID. Control data were preprocessed with Arivis' Particle Enhancement denoising function to suppress local background and enhance puncta brightness. Enhanced puncta were then segmented with the Blob Finder segmentation tool and the segments were then filtered by volume. Resulting segments were then used to measure the mean intensity of the raw unprocessed control data. Measurements were then exported and mean background values for each time point were calculated. Background volumes were then created in Fiji (v2.9.0/1.53t).

Analysis of experimental data (triple-fluorescent bradyzoites with or without IAA treatment) was subdivided into four Arivis pipelines: In pipeline 1, background volumes created in Fiji were imported and subtracted from the 488-nm channel of the experimental data. The Particle Enhancement function was applied to each channel and the Blob Finder tool was used to segment the resulting volumes. In pipeline 2, cysts were segmented using Arivis' Machine Learning Segmenter, which utilized a model that was trained on the experimental data. In pipeline 3, puncta segments generated with the Blob Finder function were filtered by volume to eliminate segments smaller than  $0.2 \mu\text{m}^3$ . The remaining puncta segments were then further filtered by their overlap (greater than 90%) as a proxy for co-occurrence of puncta segments. In pipeline 4, filtered puncta segments were then grouped based on overlap with segments from each channel. Object volumes were also calculated for puncta segments from each channel.

Per cyst, the ratio of co-occurrence was calculated from dividing the number of puncta with overlap by the total number of puncta in each channel. This accounts for the overall decreased number of puncta in the 488-nm channel observed in the IAA-treated condition due to TgATG9-mAID knockdown. The co-occurrence between TgATG9 and TgATG8 was determined by taking the number of TgATG9 puncta found to be overlapping with TgATG8 and dividing by the total number of TgATG9 present. The co-occurrence between TgATG8 and TgATG9 was determined by taking the number of TgATG8 puncta found to be overlapping with TgATG9 and dividing by the total number of TgATG8 present. The co-occurrence between TgATG9 and FYVE was determined by taking the number of TgATG9 puncta found to be overlapping with FYVE and dividing by the total number of TgATG9 present. The co-occurrence between TgATG8 and FYVE was determined by taking the number of TgATG8 puncta found to be overlapping with FYVE and dividing by the total number of TgATG8 present.

### **Bradizoite viability assay**

The viability of bradyzoites was assessed by combining plaque assay and qPCR normalization of parasite genome numbers [15,25]. *T. gondii* tachyzoites



were differentiated into bradyzoites in 6-well tissue culture plates for 7 days with daily media changes. Following differentiation, bradyzoites were treated with 500  $\mu$ M IAA or an equal volume of ethanol as a control with daily media and treatment changes for 7 days. Following the treatment period, bradyzoites were harvested by pepsin treatment (0.026% pepsin in 170 mM NaCl and 60 mM HCl, final concentration), and filtration [71]. Bradyzoites were enumerated and 500 or 2000 bradyzoites per well were added in triplicate to fresh 6-well tissue culture plates containing confluent HFFs in D10 medium. Bradyzoite-derived plaques were allowed to form undisturbed for 14 days, grown at 37°C under 5% CO<sub>2</sub>. Plaques were counted using a light microscope and plates were then stained with crystal violet fix solution (0.2% of crystal violet and 70% of EtOH) for 15 min at room temperature, rinsed with water. Next, 500  $\mu$ L of the initial pepsin-treated bradyzoites was used for genomic DNA extraction with the DNeasy Blood and Tissue Kit (Qiagen, 69506). qPCR was performed using 2  $\mu$ L of genomic DNA in SsoAdvanced<sup>TM</sup> Universal SYBR<sup>®</sup> Green Supermix (Bio-Rad, 172-5271) and primers for a 529-base pair repetitive element of *T. gondii* (forward AGGAGAGATATCAGGACTGTAG; reverse GCGTCGTCTCGTCTAGATCG) [93]. The qPCR reactions were performed with the CFX96 Touch Real-Time PCR Detection System (Bio-Rad) using the following parameters: 3 min at 98°C, and 40 cycles of 15s at 98°C, 30s at 58.5°C, and 30s at 72°C. A standard curve was built with 6.4, 32, 160, 800, 4000, 2000 parasite genomes. The number of plaques was normalized to the calculated number of genomes present in the inoculating samples.

### Statistical analyses

Data were analyzed using GraphPad prism. For each data set, outliers were identified and removed using ROUT with a Q value of 0.1%. Data were then tested for normality (D'Agostino-Pearson omnibus normality test) and equal variance. Student's *t*-tests or analysis of variance (ANOVA) tests were performed for normally distributed data with equal or assumed equal variance, when appropriate. Specific details of each test are described in the corresponding figure legends. Power analysis was not performed when the study was designed. Sample sizes were determined based on the capacity of each assay to collect sufficient values needed to support rigorous analyses and statistical tests.

### Acknowledgements

We thank the Thorner lab at the University of California, Berkeley for providing the Pgk1 antibody, the Sibley lab at Washington University in St. Louis for the TgActin antibody, and the Bradley lab at UCLA for the ATRX1 antibody. We thank the Weiss lab at Albert Einstein College of Medicine for the HaloTag plasmid. We thank

Dr. Christophe-Sebastien Arnold for helping in structural modeling of TgATG9. We thank Carruthers lab members: Dr. My-Hang Huynh, Dr. Einar Olafsson, Patrick Rimple, and Tracey Schultz for their key technical support. We thank Biorender for providing a user-friendly tool for creating schematic illustrations.

## Abbreviations

AID: auxin-inducible degron; CFUs: colony-forming units; IAA: indole-3-acetic acid; LLSM: lattice light sheet microscopy; mAID: minimal auxin-inducible degron; PLVAC: plant-like vacuolar compartment.

## Funding

This work was supported by grants from the US National Institute of Health, including R01 AI120607 (V.B.C.), R21 AI160610 (V.B.C.), T32 AI007528 (P.T.), T32 GM007863 (P.T.), F30AI169762 (P.T.), and GM131919 (D.J.K.).

## Disclosures Statement

No potential conflict of interest was reported by the author(s).

## ORCID

Daniel J. Klionsky  <http://orcid.org/0000-0002-7828-8118>

## References

1. Dubey JP. History of the discovery of the life cycle of *Toxoplasma gondii*. *Int J Parasitol*. 2009 Jul 1;39(8):877–82.
2. Montoya JG, Liesenfeld O. Toxoplasmosis. *Lancet*. 2004 Jun 12;363(9425):1965–76.
3. Saadatnia G, Golkar M. A review on human toxoplasmosis. *Scand J Infect Dis*. 2012 Nov;44(11):805–14.
4. Rougier S, Montoya JG, Peyron F. Lifelong persistence of *Toxoplasma* cysts: a Questionable Dogma? *Trends Parasitol*. 2017 Feb;33(2):93–101.
5. Layton J, Theiopoulos DC, Rutenberg D, et al. Clinical spectrum, radiological findings, and outcomes of severe toxoplasmosis in immunocompetent hosts: a systematic review. *Pathogens*. 2023 Mar 31;12(4).
6. Lijeskic O, Stajner T, Srbijanovic J, et al. Postnatal ocular toxoplasmosis in immunocompetent patients. *J Infect Dev Ctries*. 2021 Oct 31;15(10):1515–1522.
7. Alday PH, Doggett JS. Drugs in development for toxoplasmosis: advances, challenges, and current status. *Drug Des Devel Ther*. 2017;11:273–293.
8. Cerutti A, Blanchard N, Besteiro S. The bradyzoite: a key developmental stage for the persistence and pathogenesis of toxoplasmosis. *Pathogens*. 2020 Mar 21;9(3):234.

9. Ferguson DJ, Hutchison WM. An ultrastructural study of the early development and tissue cyst formation of *Toxoplasma gondii* in the brains of mice. *Parasitol Res.* [1987](#);73(6):483–91.
10. Lemgruber L, Lupetti P, Martins-Duarte ES, et al. The organization of the wall filaments and characterization of the matrix structures of *Toxoplasma gondii* cyst form. *Cell Microbiol.* [2011](#) Dec;13(12):1920–32.
11. Tu V, Mayoral J, Sugi T, et al. Enrichment and proteomic characterization of the cyst wall from *In vitro* *Toxoplasma gondii* cysts. *mBio.* 2019 Apr 30;10(2).
12. Dou Z, McGovern OL, Di Cristina M, et al. *Toxoplasma gondii* ingests and digests host cytosolic proteins. *mBio.* 2014 Jul 15;5(4):e01188–14.
13. Carruthers VB. Parasites and their heterophagic appetite for disease. *PLOS Pathog.* [2015](#) May;11(5):e1004803.
14. Kannan G, Thaprawat P, Schultz TL, et al. Acquisition of host cytosolic protein by *Toxoplasma gondii* bradyzoites. *mSphere.* 2021 Jan 27;6(1).
15. Di Cristina M, Dou Z, Lunghi M, et al. *Toxoplasma* depends on lysosomal consumption of autophagosomes for persistent infection. *Nat Microbiol.* 2017 Jun 19;2:17096.
16. Mizushima N, Komatsu M. Autophagy: renovation of cells and tissues. *Cell.* 2011 Nov 11;147(4):728–741.
17. Feng Y, He D, Yao Z, et al. The machinery of macroautophagy. *Cell Res.* [2014](#) Jan;24(1):24–41.
18. Besteiro S. Autophagy in apicomplexan parasites. *Curr Opin Microbiol.* [2017](#) Dec;40:14–20.
19. Romano PS, Akematsu T, Besteiro S, et al. Autophagy in protists and their hosts: when, how and why? *Autophagy Rep.* [2023](#);2(1).
20. Leveque MF, Berry L, Cipriano MJ, et al. Autophagy-related protein ATG8 has a noncanonical function for apicoplast inheritance in *Toxoplasma gondii*. *mBio.* 2015 Oct 27;6(6):e01446–415.
21. Cheng L, Tian Y, Wang Y, et al. *Toxoplasma* tgatg8-tgatg3 interaction primarily contributes to apicoplast inheritance and parasite growth in tachyzoite. *Microbiol Spectr.* 2022 Feb 23;10(1):e0149521.
22. Fu J, Zhao L, Pang Y, et al. Apicoplast biogenesis mediated by ATG8 requires the ATG12-ATG5-ATG16L and SNAP29 complexes in *Toxoplasma gondii*. *Autophagy.* [2023](#) Apr;19(4):1258–1276.
23. Wu M, Ying J, Lin X, et al. *Toxoplasma gondii* autophagy-related protein ATG7 maintains apicoplast inheritance by stabilizing and lipidating ATG8. *Biochim Biophys Acta Mol Basis Dis.* [2024](#) Jan;1870(1):166891.
24. Nguyen HM, El Hajj H, El Hajj R, et al. *Toxoplasma gondii* autophagy-related protein ATG9 is crucial for the survival of parasites in their host. *Cell Microbiol.* [2017](#) Jun;19(6).
25. Smith D, Kannan G, Coppens I, et al. *Toxoplasma* TgATG9 is critical for autophagy and long-term persistence in tissue cysts. *Elife.* 2021 Apr 27;10:e59384.
26. Matoba K, Kotani T, Tsutsumi A, et al. Atg9 is a lipid scramblase that mediates autophagosomal membrane expansion. *Nat Struct Mol Biol.* 2020 Oct 26;27(12):1185–1193.
27. Maeda S, Yamamoto H, Kinch LN, et al. Structure, lipid scrambling activity and role in autophagosome formation of ATG9A. *Nat Struct Mol Biol.* 2020 Oct 26;27(12):1194–1201.

28. Orii M, Tsuji T, Ogasawara Y, et al. Transmembrane phospholipid translocation mediated by Atg9 is involved in autophagosome formation. *J Cell Biol.* 2021 Mar 1;220(3):e202009194.
29. Mailler E, Guardia CM, Bai X, et al. The autophagy protein ATG9A enables lipid mobilization from lipid droplets. *Nat Commun.* 2021 Nov 19;12(1):6750.
30. Guardia CM, Tan XF, Lian T, et al. Structure of human atg9a, the only transmembrane protein of the core autophagy machinery. *Cell Rep.* 2020 Jun 30;31(13):107837.
31. Noda T, Kim J, Huang WP, et al. Apg9p/Cvt7p is an integral membrane protein required for transport vesicle formation in the Cvt and autophagy pathways. *J Cell Biol.* 2000 Feb 7;148(3):465–480.
32. Gomez-Sanchez R, Rose J, Guimaraes R, et al. Atg9 establishes Atg2-dependent contact sites between the endoplasmic reticulum and phagophores. *J Cell Biol.* 2018 Aug 6;217(8):2743–2763.
33. van Vliet AR, Chiduzza GN, Maslen SL, et al. ATG9A and ATG2A form a heteromeric complex essential for autophagosome formation. *Mol Cell.* 2022 Nov 17;82(22):4324–4339 e8.
34. Noda NN. Atg2 and Atg9: intermembrane and interleaflet lipid transporters driving autophagy. *Biochim Biophys Acta Mol Cell Biol Lipids.* 2021 Aug;1866(8):158956.
35. Webber JL, Young AR, Tooze SA. Atg9 trafficking in Mammalian cells. *Autophagy.* 2007 Jan-Feb;3(1):54–56.
36. Mari M, Reggiori F. Atg9 trafficking in the yeast *Saccharomyces cerevisiae*. *Autophagy.* 2007 Mar-Apr;3(2):145–148.
37. Holzer E, Martens S, Tulli S. The role of atg9 vesicles in autophagosome biogenesis. *J Mol Biol.* 2024 Feb 10:168489.
38. Imai K, Hao F, Fujita N, et al. Atg9A trafficking through the recycling endosomes is required for autophagosome formation. *J Cell Sci.* 2016 Oct 15;129(20):3781–3791.
39. Yamamoto H, Kakuta S, Watanabe TM, et al. Atg9 vesicles are an important membrane source during early steps of autophagosome formation. *J Cell Biol.* 2012 Jul 23;198(2):219–233.
40. Olivas TJ, Wu Y, Yu S, et al. ATG9 vesicles comprise the seed membrane of mammalian autophagosomes. *J Cell Biol.* 2023 Jul 3;222(7).
41. Sawa-Makarska J, Baumann V, Coudeville N, et al. Reconstitution of autophagosome nucleation defines Atg9 vesicles as seeds for membrane formation. *Science.* 2020 Sep 4;369(6508).
42. Karanasios E, Walker SA, Okkenhaug H, et al. Autophagy initiation by ULK complex assembly on ER tubulovesicular regions marked by ATG9 vesicles. *Nat Commun.* 2016 Aug 11;7:12420.
43. Zhuang X, Chung KP, Cui Y, et al. ATG9 regulates autophagosome progression from the endoplasmic reticulum in *Arabidopsis*. *Proc Natl Acad Sci USA.* 2016 Jan 17;114(3):E426–E435.
44. Vargas Duarte P, Reggiori F. The organization and function of the phagophore-er membrane contact sites. *Contact (Thousand Oaks).* 2023 Jan-Dec ;6:25152564231183898.
45. Claude-Taupin A, Jia J, Bhujabal Z, et al. ATG9A protects the plasma membrane from programmed and incidental permeabilization. *Nat Cell Biol.* 2021 Aug;23(8):846–858.

46. Abramson J, Adler J, Dunger J, et al. Accurate structure prediction of biomolecular interactions with AlphaFold 3. *Nature*. 2024 Jun;630(8016):493–500.
47. He C, Baba M, Cao Y, et al. Self-interaction is critical for Atg9 transport and function at the phagophore assembly site during autophagy. *Mol Biol Cell*. 2008 Dec;19(12):5506–5516.
48. He C, Song H, Yorimitsu T, et al. Recruitment of Atg9 to the preautophagosomal structure by Atg11 is essential for selective autophagy in budding yeast. *J Cell Biol*. 2006 Dec 18;175(6):925–935.
49. Feng Y, Backues SK, Baba M, et al. Phosphorylation of Atg9 regulates movement to the phagophore assembly site and the rate of autophagosome formation. *Autophagy*. 2016;12(4):648–658.
50. Reggiori F, Tucker KA, Stromhaug PE, et al. The Atg1-Atg13 complex regulates Atg9 and Atg23 retrieval transport from the pre-autophagosomal structure. *Dev Cell*. 2004 Jan;6(1):79–90.
51. Yen WL, Legakis JE, Nair U, et al. Atg27 is required for autophagy-dependent cycling of Atg9. *Mol Biol Cell*. 2007 Feb;18(2):581–593.
52. Noda T, Klionsky DJ. The quantitative Pho8Delta60 assay of nonspecific autophagy. *Methods Enzymol*. 2008;451:33–42.
53. Nair U, Thumm M, Klionsky DJ, et al. GFP-Atg8 protease protection as a tool to monitor autophagosome biogenesis. *Autophagy*. 2011 Dec;7(12):1546–50.
54. Noda T. Viability assays to monitor yeast autophagy. *Methods Enzymol*. 2008;451:27–32.
55. Suzuki SW, Onodera J, Ohsumi Y. Starvation induced cell death in autophagy-defective yeast mutants is caused by mitochondria dysfunction. *PLOS ONE*. 2011 Feb 25;6(2):e17412.
56. Feng Y, Ariosa AR, Yang Y, et al. Downregulation of autophagy by Met30-mediated Atg9 ubiquitination. *Proc Natl Acad Sci USA*. 2021 Jan 5;118(1).
57. Gajria B, Bahl A, Brestelli J, et al. ToxoDB: an integrated *Toxoplasma gondii* database resource. *Nucleic Acids Res*. 2008 Jan;36(Database issue):D553–556.
58. Treeck M, Sanders JL, Elias JE, et al. The phosphoproteomes of *Plasmodium falciparum* and *Toxoplasma gondii* reveal unusual adaptations within and beyond the parasites' boundaries. *Cell Host Microbe*. 2011 Oct 20;10(4):410–419.
59. Klappan AK, Hones S, Mylonas I, et al. Proteasome inhibition by quercetin triggers macroautophagy and blocks mTOR activity. *Histochem Cell Biol*. 2012 Jan;137(1):25–36.
60. Chan LL, Shen D, Wilkinson AR, et al. A novel image-based cytometry method for autophagy detection in living cells. *Autophagy*. 2012 Sep;8(9):1371–82.
61. Miyayama T, Fujiki K, Matsuoka M. Silver nanoparticles induce lysosomal-autophagic defects and decreased expression of transcription factor EB in A549 human lung adenocarcinoma cells. *Toxicol In Vitro*. 2018 Feb;46:148–154.
62. Zhang L, Yang H, Duan X, et al. Modulation of autophagy affected tumorigenesis induced by the envelope glycoprotein of JSRV. *Virology*. 2024 Jun;594:110059.
63. Larson ET, Parussini F, Huynh MH, et al. *Toxoplasma gondii* cathepsin L is the primary target of the invasion-inhibitory compound morpholinurea-leucyl-homophenyl-vinyl sulfone phenyl. *J Biol Chem*. 2009 Sep 25;284(39):26839–50.

64. Brown KM, Long S, Sibley LD. Conditional knockdown of proteins using auxin-inducible degron (AID) fusions in *Toxoplasma gondii*. *Bio Protoc*. 2018 Feb 20;8(4):e2728.
65. Licon MH, Giuliano CJ, Chan AW, et al. A positive feedback loop controls *Toxoplasma* chronic differentiation. *Nat Microbiol*. 2023 May;8(5):889–904.
66. Daher W, Morlon-Guyot J, Sheiner L, et al. Lipid kinases are essential for apicoplast homeostasis in *Toxoplasma gondii*. *Cell Microbiol*. 2015 Apr;17(4):559–78.
67. Piro F, Masci S, Kannan G, et al. A *Toxoplasma gondii* putative amino acid transporter localizes to the plant-like vacuolar compartment and controls parasite extracellular survival and stage differentiation. *mSphere*. 2024 Jan 30;9(1):e0059723.
68. Chen BC, Legant WR, Wang K, et al. Lattice light-sheet microscopy: imaging molecules to embryos at high spatiotemporal resolution. *Science*. 2014 Oct 24;346(6208):1257998.
69. Ganter M, Frischknecht F. Illuminating *Plasmodium* invasion by lattice-light-sheet microscopy. *Trends Parasitol*. 2021 Sep;37(9):777–779.
70. Mannino PJ, Perun A, Surovstei I, et al. A quantitative ultrastructural timeline of nuclear autophagy reveals a role for dynamin-like protein 1 at the nuclear envelope. *bioRxiv*. 2024 Feb 15. 02.14.580336.
71. Mayoral J, Di Cristina M, Carruthers VB, et al. *Toxoplasma gondii*: Bradyzoite Differentiation In Vitro and In Vivo. *Methods Mol Biol*. 2020;2071:269–282.
72. Altschul SF, Gish W, Miller W, et al. Basic local alignment search tool. *J Mol Biol*. 1990 Oct 5;215(3):403–10.
73. Chumpen Ramirez S, Gomez-Sanchez R, Verlhac P, et al. –Atg9 interactions via its transmembrane domains are required for phagophore expansion during autophagy. *Autophagy*. 2023 May;19(5):1459–1478.
74. Papinski D, Schuschnig M, Reiter W, et al. Early steps in autophagy depend on direct phosphorylation of Atg9 by the Atg1 kinase. *Mol Cell*. 2014 Feb 6;53(3):471–83.
75. Broadbent DG, Barnaba C, Perez GI, et al. Quantitative analysis of autophagy reveals the role of ATG9 and ATG2 in autophagosome formation. *J Cell Biol*. 2023 Jul 3;222(7):e202210078.
76. Yesbolatova A, Saito Y, Kitamoto N, et al. The auxin-inducible degron 2 technology provides sharp degradation control in yeast, mammalian cells, and mice. *Nat Commun*. 2020 Nov 11;11(1):5701.
77. Ye S, Lunghi M, Soldati-Favre D. A Signaling factor linked to *Toxoplasma gondii* guanylate cyclase complex controls invasion and egress during acute and chronic infection. *mBio*. 2022 Oct 26;13(5):e0196522.
78. Macdonald L, Taylor GC, Brisbane JM, et al. Rapid and specific degradation of endogenous proteins in mouse models using auxin-inducible degrons. *Elife*. 2022 Jun 23; 11.
79. Tomita T, Bzik DJ, Ma YF, et al. The *Toxoplasma gondii* cyst wall protein CST1 is critical for cyst wall integrity and promotes bradyzoite persistence. *PLOS Pathog*. 2013;9(12):e1003823.
80. Uboldi AD, McCoy JM, Blume M, et al. Regulation of starch stores by a  $Ca^{2+}$ -dependent protein kinase is essential for viable cyst development in *Toxoplasma gondii*. *Cell Host Microbe*. 2015 Dec 9;18(6):670–81.

81. Sugi T, Tu V, Ma Y, et al. *Toxoplasma gondii* requires glycogen phosphorylase for balancing amylopectin storage and for efficient production of brain Cysts. *mBio*. 2017 Aug 29;8(4).
82. Sanchez SG, Bassot E, Cerutti A, et al. The apicoplast is important for the viability and persistence of *Toxoplasma gondii* bradyzoites. *Proc Natl Acad Sci USA*. 2023 Aug 22;120(34):e2309043120.
83. Meng EC, Goddard TD, Pettersen EF, et al. UCSF ChimeraX: Tools for structure building and analysis. *Protein Sci*. 2023 Nov;32(11):e4792.
84. Robinson JS, Klionsky DJ, Banta LM, et al. Protein sorting in *Saccharomyces cerevisiae*: isolation of mutants defective in the delivery and processing of multiple vacuolar hydrolases. *Mol Cell Biol*. 1988 Nov;8(11):4936–48.
85. Mao K, Chew LH, Yip CK, et al. The role of Atg29 phosphorylation in PAS assembly. *Autophagy*. 2013 Dec;9(12):2178–2179.
86. Jin M, He D, Backues SK, et al. Transcriptional regulation by Pho23 modulates the frequency of autophagosome formation. *Curr Biol*. 2014 Jun 16;24(12):1314–1322.
87. Gueldener U, Heinisch J, Koehler GJ, et al. A second set of loxP marker cassettes for Cre-mediated multiple gene knockouts in budding yeast. *Nucleic Acids Res*. 2002 Mar 15;30(6):e23.
88. Cheong H, Klionsky DJ. Biochemical methods to monitor autophagy-related processes in yeast. *Methods Enzymol*. 2008;451:1–26.
89. Weiss LM, Laplace D, Takvorian PM, et al. A cell culture system for study of the development of *Toxoplasma gondii* bradyzoites. *J Eukaryot Microbiol*. 1995 Mar-Apr;42(2):150–7.
90. Di Cristina M, Carruthers VB. New and emerging uses of CRISPR/Cas9 to genetically manipulate apicomplexan parasites. *Parasitology*. 2018 Aug;145(9):1119–1126.
91. Smith TA, Lopez-Perez GS, Herneisen AL, et al. Screening the *Toxoplasma* kinome with high-throughput tagging identifies a regulator of invasion and egress. *Nat Microbiol*. 2022 Jun;7(6):868–881.
92. Schindelin J, Arganda-Carreras I, Frise E, et al. Fiji: an open-source platform for biological-image analysis. *Nat Methods*. 2012 Jun 28;9(7):676–682.
93. Reischl U, Bretagne S, Kruger D, et al. Comparison of two DNA targets for the diagnosis of Toxoplasmosis by real-time PCR using fluorescence resonance energy transfer hybridization probes. *BMC Infect Dis*. 2003 May 2;3:7.